Article

Rapid Preparation of (BiO)$_2$CO$_3$ Nanosheets by Microwave-Assisted Hydrothermal Method with Promising Photocatalytic Activity Under UV-Vis Light

Juliane Z. Marinho,[a] Lidiaine M. Santos,[a] Leilane R. Macario,[b] Elson Longo,[b] Antonio E. H. Machado,[a,c] Antonio O. T. Patrocinio[a] and Renata C. Lima*,[a]

[a]*Instituto de Química, Universidade Federal de Uberlândia, CP 593, 38400-902 Uberlândia-MG, Brazil*

[b]*Instituto de Química, Universidade Estadual Paulista, 14800-900 Araraquara-SP, Brazil*

[c]*Departamento de Química, Universidade Federal de Goiás, Campus Catalão, 75704-020 Catalão-GO, Brazil*

Crystalline (BiO)$_2$CO$_3$ nanosheets were synthesized by a rapid one-step reaction via microwave-assisted hydrothermal method using urea as a morphology mediator and carbon source. The hydrothermal method combined with microwave heating allowed to obtain sheet-like (BiO)$_2$CO$_3$ particles at shorter reaction times when compared to the conventional heating hydrothermal method. The photocatalytic activity of the as prepared samples was evaluated towards degradation of Ponceau 4R (C.I. 16255) under artificial UV-Vis light irradiation. The results show that good photocatalytic efficiency can be obtained for powders prepared with reaction times as low as 2 minutes.

Keywords: (BiO)$_2$CO$_3$, nanosheets, microwave-assisted hydrothermal method, photocatalysis

Introduction

Over the past decade, considerable efforts have been made to synthesize nanostructures for organic pollutant degradation under UV and visible-light irradiation.[1-4] Bare and doped anatase TiO$_2$ structure, the most commonly used photocatalyst, has shown excellent results on complete mineralization of pollutants as well as in devices for effective solar energy conversion.[5-12] From the first report by Fujishima and Honda[13] on water-splitting using TiO$_2$ and UV light, considerable attention have been deposited on the synthesis of low dimensional nanomaterials capable of realize photocatalysis.[14-19] Given the interest in semiconductor photocatalysts for environmental applications, it is necessary to develop new materials with improved visible-light-response in order to efficiently use the solar energy.

Typical Aurivillius oxides such as Bi$_2$MO$_6$ (M = W, Mo), BiVO$_4$, BiOX (X = Cl, Br) and Bi$_2$O$_3$ have shown excellent photocatalytic activity for both, solar energy conversion and environmental remediation.[20-25] Zhang *et al.*[26] reported the effect of morphology and variation in local structure on Bi$_2$MoO$_6$ photocatalytic activities at different pHs.

Ren *et al.*[27] investigated the different BiVO$_4$ microstructures and their photocatalytic activities for the degradation of rhodamine B under visible light. Yu *et al.*[28] showed different photocatalytic performances of Bi$_2$WO$_6$ powders in the degradation of organic pollutants depending on their calcination temperatures. Bismuth compounds with perovskite structure, such as BiFeO$_3$, also present photocatalysis applications.[29]

Bismuth subcarbonate ((BiO)$_2$CO$_3$) Aurivillius structured was firstly reported by Grice research group.[30] This oxy-carbonate has an alternate intergrown Bi$_2$O$_2$$^{2+}$ and CO$_3$$^{2-}$ layers in which the plane of the CO$_3$$^{2-}$ ions is orthogonal to the one of the Bi−O bond. Moreover, the internal layered structure of (BiO)$_2$CO$_3$ could guide the lower growth along (001) axis and thus morphologies like nanosheets or nanoplates can be obtained.[31-33] (BiO)$_2$CO$_3$ with layered structure has presented expressive antibacterial[34] and photocatalytic[35-38] properties.

The size and morphology are important factors in the photocatalytic activity and so is attractive to develop methods to prepare bismuth-based compounds with controlled size and shape. In particular, by the hydrothermal method combined with microwave heating, inorganic compounds can be obtained in short reaction times, low temperatures, low power consumption, no air pollution

*e-mail: rclima@iqufu.ufu.br

and can also easily screen a wide range of experimental conditions in order to optimize the material preparation and properties.[39-44]

Herein, we report the $(BiO)_2CO_3$ nanosheets prepared by a rapid one-step reaction using the microwave-assisted hydrothermal (MAH) method. Their photocatalytic properties towards the degradation of the organic dye Ponceau 4R under artificial UV-Vis light irradiation were investigated and compared of $(BiO)_2CO_3$ prepared by other methods. The azo-dye Ponceau 4R was chose due its large use in the food industry in Brazil,[45] despite the fact of several countries, including the United States, Norway and Finland, its classified as a carcinogen.[46,47] Moreover, several works in the literature have described the photocatalytic activities of new materials against azo compounds.[48-50] The synthetic methodology used allows a rapid and uniform heating of particles, leading to the production of efficient photocatalysts at short reaction times.

Experimental

Synthesis of $(BiO)_2CO_3$ nanostructures

All chemicals were analytical grade and were used without further purifications. 1.0×10^{-3} mol of $Bi(NO_3)_3 \cdot 5H_2O$ was dissolved in concentrated nitric acid under constant stirring. 40 mL of distilled water with 5×10^{-3} mol of urea were added to the solution and the pH was adjusted to 9 using a 3 mol L^{-1} KOH solution. The suspension was transferred to a 50 mL Teflon autoclave and heated in 800 W microwave at 130 ºC during 2 and 8 min. The pale yellow solid obtained was washed with distilled water and ethanol and dried at 60 ºC.

Characterization

Crystalline phases were determined using a Shimadzu X-ray diffraction (XRD) 6000 equipped with CuK radiation ($\lambda = 1.5406$ Å) in the 2θ range from 10° to 60° with 0.02° *per* min scan increment. Scanning electron microscopy with a field emission gun (FE-SEM) Supra 35-VP was used to investigate particle size and morphology. The diffuse reflectance absorption spectra of the powders were recorded at room temperature on a Shimadzu UV-1650PC spectrophotometer equipped with an integrating sphere, in the region between 190 and 850 nm. Potassium bromide was used as reference in these experiments. The infrared spectra was measured from powder samples diluted in potassium bromide on a FTIR Shimadzu IR-Prestige 21 spectrometer in the 400-4000 cm^{-1} region. Raman spectra was recorded on a RFS/100/S Bruker Fourier Transform Raman (FT-Raman) spectrometer. The 1064 nm line of a Nd:YAG ion laser was used as the excitation source.

Photocatalytic studies

The photocatalytic activity of the new $(BiO)_2CO_3$ nanostructures were evaluated against the degradation of the commercial dye Ponceau 4R, P4R (acid red 18, C.I. 16255, Sigma-Aldrich, 80% dye content), under UV-Vis irradiation. The photocatalytic experiments were carried out in water cooled reactor described in detail previously.[6] A 400 W high pressure mercury lamp was used as irradiation source to provide a photonic flux of c.a. 3.3×10^6 Einsteins s^{-1}. 100 mg mL^{-1} of the catalyst was added to 125 mg mL^{-1} P4R aqueous solution (pH = 6.1) under magnetic stirring (4 L irradiated volume). The mixture was irradiated during 120 minutes. The system was kept at 40 ± 2 ºC. Aliquots were taken at 20 minutes intervals, filtered and analyzed spectrophotometrically, following the bleaching at 507 nm.[6] The results presented are averages of at least three different experiments. Control measurements in the dark were performed and no dye adsorption at the catalyst surface was observed.

Results and Discussion

In the Figure 1 are shown the X-ray diffraction patterns of the powders obtained using the microwave-assisted hydrothermal (MAH) method with 2 or 8 minutes heating. The diffraction peaks can be indexed to the tetragonal $(BiO)_2CO_3$ structure with lattice constants, a = b = 3.865 Å, c = 13.675 Å and space group I$_4$/mmm, which are consistent with the standard card, JCPDS No. 41-1488. The sharp and intense peaks indicated the highly crystalline nature of the $(BiO)_2CO_3$ samples obtained over 2 and 8 min using the MAH conditions. Results obtained by Rietveld refinement of the XRD patterns of the samples show the presence of small amounts of secondary phases relative to polymorphs of bismuth oxides (Bi_2O_3) mixture and the principal tetragonal $(BiO)_2CO_3$ phase with 99.9% and 81.3% to the samples obtained after 2 and 8 min by MAH method (Supplementary Information). In addition, the intensity ratio of the (110) peak to the (013) is about 0.42, higher than the correspondent standard card of bismutite, indicating that the crystals have anisotropic growth along the (110) plane.[37]

The morphology of the samples observed by FE-SEM is shown in Figure 2. The 2 min heated $(BiO)_2CO_3$ powders exhibits irregular morphology with aggregates of thin sheet-like particles as shown in Figure 2a. As the reaction time is increased to 8 min, one can observe well-defined
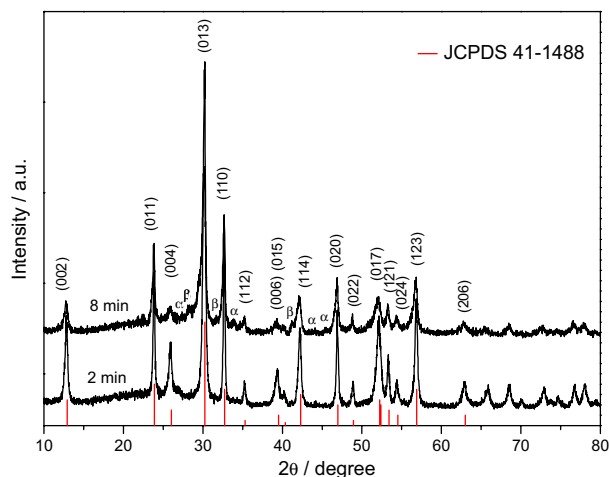
Figure 1. X-ray diffraction patterns of $(BiO)_2CO_3$ obtained by MAH method.

two-dimensional (2D) nanosheets of fairly homogeneous thickness of about 10 nm, as shown in Figure 2b (inset).

During the heating into autoclave the prolonged urea hydrolysis results in either CO_2 in acidic medium or to CO_3^{2-} ions in basic medium.[51] Under hydrothermal conditions the concentration of urea and the reaction time are important factors influencing the particles growth and the morphology of the products.[52] The hydrothermal method combined with microwave heating can accelerate the kinetics of crystallization by one to two orders of magnitude compared to the conventional hydrothermal method,[39,53] which leads to an anisotropic crystal growth and crystallization of $(BiO)_2CO_3$ under mild time and temperature conditions.

In the MAH process at high pH,[54] $Bi(NO_3)_2$ and urea are hydrolyzed to yield BiO^+ and CO_3^{2-}, respectively, that react between themselves to produce $(BiO)_2CO_3$ agglomerates. At short reaction times, the intense and homogeneous microwave heating leads to the production of crystalline but non-ordered agglomerates, Figure 2a. As the reaction time increases, a series of redissolution and recrystalyzation

steps take place, and the resulting powder exhibits regular and ordered shape as well as crystallinity. Thus, the nucleation and growth of the regular nanosheets observed in Figure 2b is likely dependent on the reaction time. In Figure 3 the effect of reaction time on the morphology of MAH synthesized $(BiO)_2CO_3$ is illustrated.

The MAH $(BiO)_2CO_3$ particles exhibit broad absorbance bands in the UV-Vis region (Figure 4). The abrupt decay of the absorbance between 380 and 420 nm is attributed to the band gap transition. The Kubelka-Munk function was used to estimate the optical absorption edge energy[55] (Figure 4, inset). The as determined band gap energy are 2.9 and 2.7 eV for $(BiO)_2CO_3$ samples obtained at 2 and 8 min heating, respectively and can be considered experimentally similar. These gap values are slightly smaller than the reported by Liu *et al.*[32] using first-principle calculations, but higher than the value reported by Zhang *et al.*[56] (2.23 eV). Such difference can probably be related to the presence of defects in the crystalline structure of the synthesized samples and also to the influence of Bi_2O_3 phases that exhibit lower band gaps[57] and could explain the low lying absorption features observed.

The infrared spectra of $(BiO)_2CO_3$ samples are shown in Figure 5. Strong absorption bands of vibrational modes of the CO_3^{2-} group are observed at 1386 and 1469 cm^{-1} assigned to anti-symmetric vibration ν_3 and 823 and 845 cm^{-1} relative to out of plane bending mode ν_2, being at 845 cm^{-1} band characteristic of $(BiO)_2CO_3$.[58] In addition, two weak absorption bands at 1064 and 670-690 cm^{-1} are ascribed to the symmetric stretching ν_1 and in-plane deformation ν_4 modes of the carbonate ion; vibration peaks at 1754 and 1731 cm^{-1} are observed for both samples.[59] Two sharp absorption bands at around 3447 and 1635 cm^{-1} can be attributed to the O−H stretching mode and bending modes of adsorbed water molecules, respectively.[58] The medium strong band at 553 cm^{-1} is assigned to the metal-oxygen bonds, Bi−O of $(BiO)_2CO_3$.
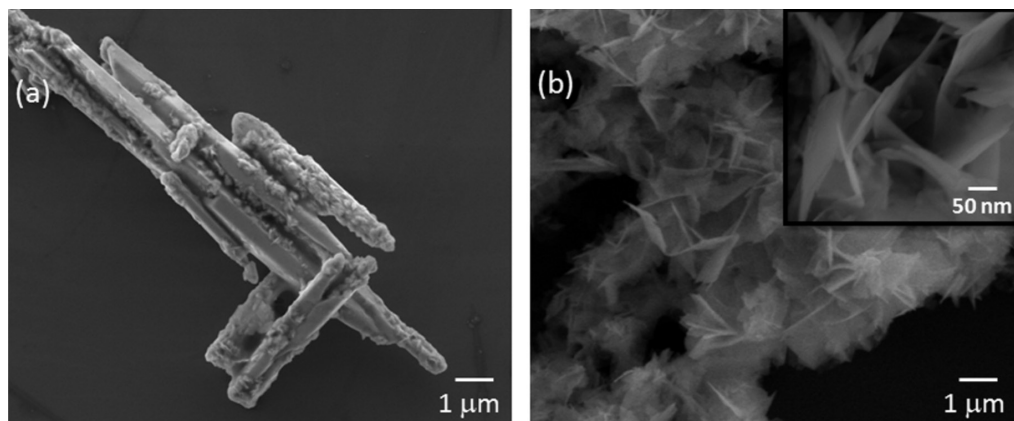
Figure 2. FE-SEM images of $(BiO)_2CO_3$ obtained by MAH method with 2 min (a) and 8 min (b) heating time.
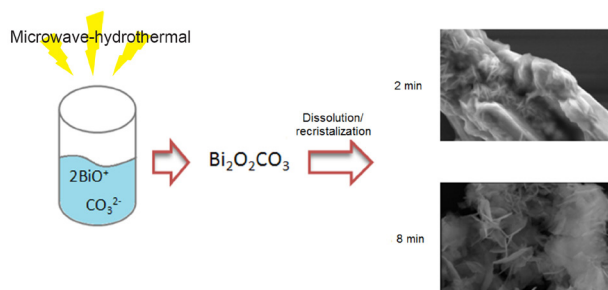
Figure 3. Scheme of rapid $(BiO)_2CO_3$ nanosheets formation by the microwave-assisted hydrothermal (MAH) method.
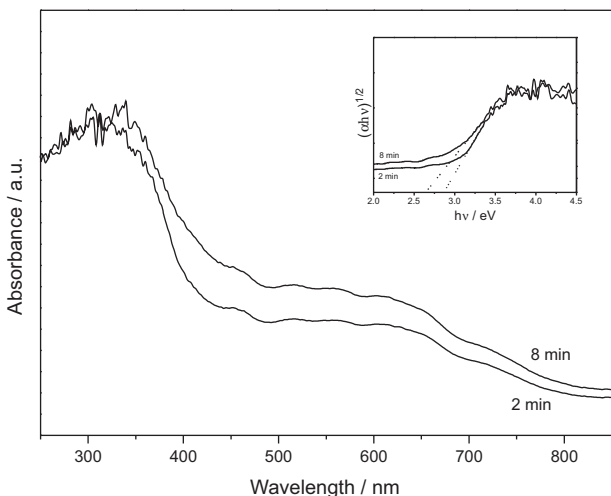
Figure 4. UV-Vis spectra of the $(BiO)_2CO_3$ nanostructures. The inset shows plots of $(\alpha h\nu)^{1/2}$ *versus* photon energy $(h\nu)$ for the $(BiO)_2CO_3$ samples.
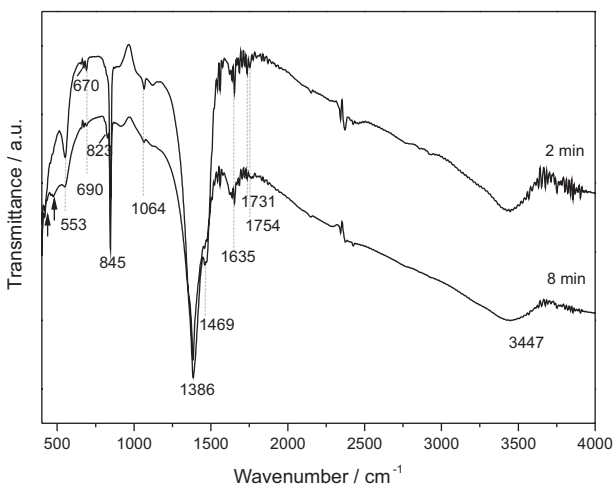
Figure 5. FT-IR spectra of $(BiO)_2CO_3$ obtained by MAH method.

The bands ascribed to the Bi−O−Bi stretching vibrations relative to Bi_2O_3 impurities are covered by the band centered at 553 cm^{-1}. The peaks at low frequencies, at 420 and 474 are characteristic to the vibration of Bi−O bonds of monoclinic α-Bi_2O_3.[60,61]

Figure 6 shows the Raman spectra of $(BiO)_2CO_3$ samples obtained by MAH method. A shoulder at

162 cm^{-1} and bands around of 360 and 668 cm^{-1} assigned to the lattice vibrations were observed. The weak band at 360 cm^{-1} is probably arise from the motion of oxygen atoms in the polymeric $(BiO)_n^{n+}$ cation.[62,63] The $(BiO)_2CO_3$ tetragonal lattice, as shown by X-ray diffraction, could only contained the CO_3^{2-} ions in orientations parallel to the (110) planes, since other dispositions result in exceedingly close inter-anionic contacts. The band at 229 and 307 cm^{-1} attributed to internal stretching modes of Bi−O bonds of β-Bi_2O_3 tetragonal structure[61] is covered by the broad band centered at 162 cm^{-1} referring to the presence of the secondary phases identified by Rietveld refinement. Bands characteristic of monoclinic α-Bi_2O_3 at 89 and 122 cm^{-1} are more pronounced for the sample obtained for 8 min heating, which contains a higher concentration of Bi_2O_3 impurities when compared to the sample prepared in 2 min.[64]
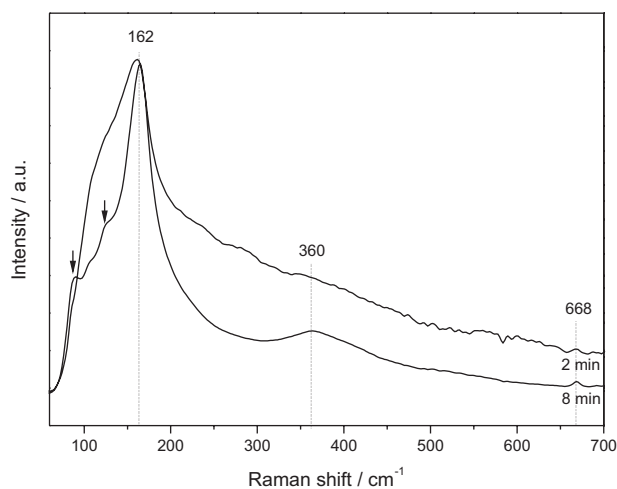
Figure 6. Raman spectra of the $(BiO)_2CO_3$ obtained by MAH method.

The photocatalytic activities of the MAH $(BiO)_2CO_3$ were evaluate against the degradation of the commercial dye Ponceau 4R (P4R). Continuous irradiation of P4R aqueous solutions in the presence of the catalysts lead to a progressive bleaching of the dye absorption band (Figure 7). As can be observed in Figure 7 (inset), no other bands appear in the spectral region monitored, indicating that no new chromophore groups have being formed during the dye degradation.

After 120 min irradiation, 43% discoloration was reached for the 2 minutes heated sample, and 40% for the sample heated during 8 minutes, which is lower than the observed for commercial TiO_2 P25 under the same conditions, but considerably higher in relation to the photo-discoloration of the dye in the absence of a catalyst.[6] The discoloration follows a pseudo first-order kinetics in relation to the organic substrate (Figure 8) which agree with the Langmuir-Hinschelwood model.[6,7,65] The rate constants
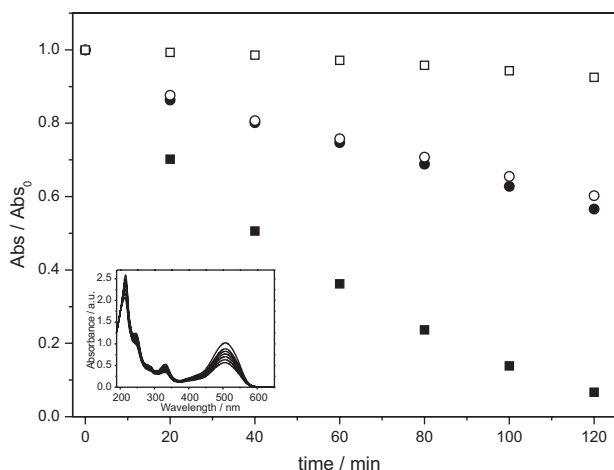
Figure 7. Absorption changes during the photocatalytic degradation of P4R, mediated by (BiO)₂CO₃ nanostructures heated by 2 min (●) and 8 min (○), obtained by the MAH method. The photocatalytic activities were compared to that for the commercial TiO₂ P25 (■) under the same conditions and also to the direct photolysis of the dye in the absence of catalyst (□). Inset: electronic spectra of P4R at different irradiation times ($\Delta t = 20$ min).

are 4.1×10^{-3} min^{-1} and 5.0×10^{-3} min^{-1}, respectively for the 2 and 8 min heated MAH (BiO)₂CO₃ samples.

The results show that the photocatalytic activities of both samples are very similar, despite the different morphologies observed by electron microscopy. Moreover, the results are in the same order of previous reported photocatalytic activities for (BiO)₂CO₃ nanosheets (Table 1). It is worthwhile to note the efficacy of the MAH method in produce this material in softer conditions and at shorter reaction times than the conventional hydrothermal method.

The small influence of the (BiO)₂CO₃ morphology on the photocatalytic behavior, for the samples prepared by the MAH method at 2 or 8 minutes of heating time, can be related to the nature of the dye employed in this study. It is well known that the catalytic process involves dye adsorption/desorption on catalyst surface. Thus, high specific surface area as well as an open porous structure should enhance the catalytic activity. The 8 min MAH (BiO)₂CO₃ is constituted by regular nanosheets well
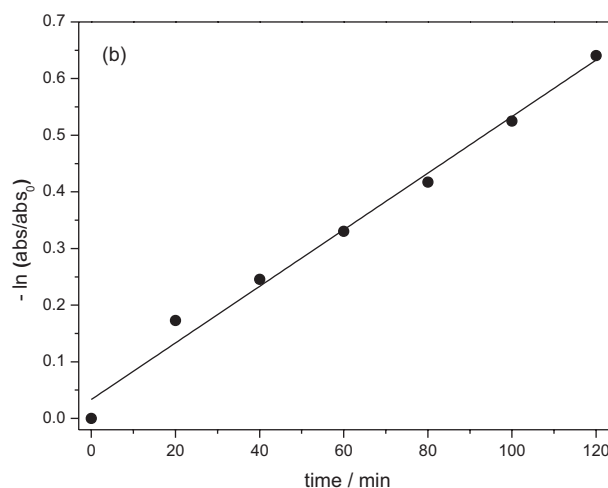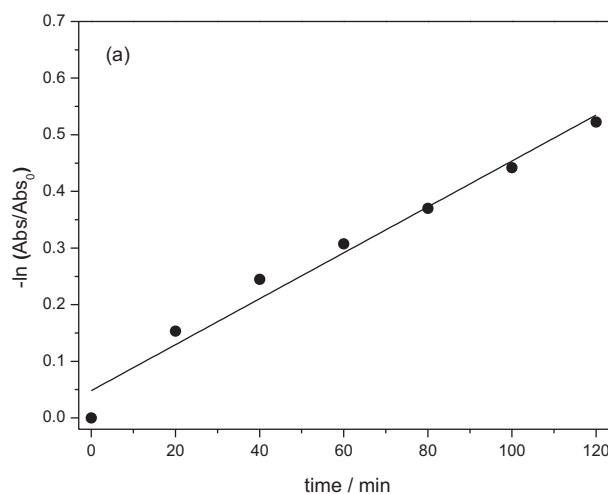
Figure 8. P4R discoloration mediated by (BiO)₂CO₃ catalysts prepared by microwave heating for 2 min (a) and 8 min (b), fitted according to a pseudo-first order kinetics.

separated from each other, while the 2 min heated sample exhibit large agglomerates. Thus, the adsorption sites should be more available in the samples heated by 8 min. However, such a change in the morphology did not result in an increase in the P4R degradation, probably due to the size of the dye that inhibits the interaction with part of the catalytic sites. Probably, the photoprocess is limited by the charge separation efficiency of the semiconductor

Table 1. Bismuth subcarbonate (BiO)₂CO₃ sheet-like nanostructures obtained under different synthesis conditions and pollutants studied

Method	Synthesis conditions	Dye	Discoloration	Rate constant k / min^{-1}	Ref.
Conventional hydrothermal	180 °C / 24 h	RhB	47% in 60 min	-	31
	180 °C / 24 h	RhB	60% in 50 min	-	66
	200 °C / 2 h	RhB	40% in 100 min	-	32
	180 °C / 24 h	RhB	35% in 120 min	0.0030	18
Microwave-hydrothermal	130 °C / 2 min	P4R	43% in 120 min	0.0044	This work
	130 °C / 8 min	P4R	40% in 120 min	0.0035	

RhB= Rhodamine B; P4R= Ponceau 4R.

and, the dye adsorption is controlled by physicochemical parameters, such as pH. Nevertheless, the higher rate constant observed for the 8 min heated sample evidences the effect of the more porous structure.

It is also important to consider the influence of secondary phases on the photocatalytic activity. These impurities can act as electron/hole traps, changing the charge recombination rates and, consequently, the photocatalytic activities. Cai *et al.*[67] have shown enhanced photocatalytic activities for β-Bi_2O_3/$Bi_2O_2CO_3$ composites in relation to pure $Bi_2O_2CO_3$, which were attributed to formation of efficient heterojunctions. As the Rietveld refinement have shown the presence of secondary phases on the MAH $Bi_2O_2CO_3$ nanosheets, similar behavior can also be occurring here and can be matter of future studies.

The absence of dye adsorption at the experimental conditions employed evidences that the negatively charged sulfonate groups present in P4R did not favor an effective adsorption of dye on the catalyst surface. Hence, better photocatalytic activity can be obtained for smaller molecules and/or at different pH. Nevertheless, the MAH $(BiO)_2CO_3$ particles can be prepared faster and in softer conditions than other catalysts reported in literature. Further studies are in progress to enhance the photocatalytic activity.

Conclusions

The microwave-assisted hydrothermal (MAH) is an appropriated, facile and environmentally friendly method for preparing rapidly $(BiO)_2CO_3$ nanosheets with controllable shape and size. The hydrothermal conditions under microwave heating accelerates the kinetics of $(BiO)_2CO_3$ crystallization and this material can be obtained at short reaction times when compared with the conventional hydrothermal method. Furthermore, the MAH conditions associated to the urea concentration play an important role on the morphology of the samples obtained. The microwave-hydrothermal time is a key factor to produce pure $(BiO)_2CO_3$ nanosheets. The as-prepared $(BiO)_2CO_3$ nanosheets obtained after 2 min and 8 min under MAH presented good photocatalytic activity for degradation of P4R under UV-Vis light, which motivates us to develop photocatalytic bismuth oxides and nanocomposites using the MAH method for degrading organic pollutants under solar light irradiation.

Supplementary Information

Supplementary data are available free of charge at http://jbcs.sbq.org.br as PDF file.

References

1. Hoffmann, M. R.; Martin, S. T.; Choi, W.Y.; Bahnemann, D. W.; *Chem. Rev.* **1995**, *95*, 69.

2. Mills, A.; LeHunte, S.; *J. Photochem. Photobiol., A* **1997**, *108*, 1.

3. Papoulis, D.; Komarneni, S.; Panagiotaras, D.; Stathatos, E.; Toli, D.; Christoforidis, K. C.; Fernandez-Garcia, M.; Li, H.; Yin, S.; Sato, T.; Katsuki, H.; *Appl. Catal. B: Environ.* **2013**, *132*, 416.

4. Li, W. J.; Li, D. Z.; Meng, S. G.; Chen, W.; Fu, X. Z.; Shao, Y.; *Environ. Sci. Technol.* **2011**, *45*, 2987.

5. Stylidi, M.; Kondarides, D. I.; Verykios, X. E.; *Appl. Catal. B: Environ.* **2004**, *47*, 189.

6. Oliveira, D. F. M.; Batista, P. S.; Muller Jr., P. S.; Velani, V.; França, M. D.; de Souza, D. R.; Machado, A. E. H.; *Dyes Pigments* **2012**, *92*, 563.

7. Machado, A. E. H.; Franca, M. D.; Velani, V.; Magnino, G. A.; Velani, H. M. M.; Freitas, F. S.; Muller, P. S.; Sattler, C.; Schmucker, A.; *Inter. J. Photoenergy* **2008**, *2008*, 1.

8. Patrocinio, A. O. T.; El-Bacha, A. S.; Paniago, E. B.; Paniago, R. M.; Iha, N. Y. M.; *Inter. J. Photoenergy* **2012**, *2012*, 1.

9. Brennaman, M. K.; Patrocinio, A. O. T.; Song, W. J.; Jurss, J. W.; Concepcion, J. J.; Hoertz, P. G.; Traub, M. C.; Iha, N. Y. M.; Meyer, T. J.; *ChemSusChem* **2011**, *4*, 216.

10. Zhang, H.; Zong, R. L.; Zhao, J. C.; Zhu, Y. F.; *Environ. Sci. Technol.* **2008**, *42*, 3803.

11. Patrocinio, A. O. T.; Paniago, E. B.; Paniago, R. M.; Iha, N. Y. M.; *Appl. Surf. Sci.* **2008**, *254*, 1874.

12. Feil, A. F.; Migowski, P.; Scheffer, F. R.; Pierozan, M. D.; Corsetti, R. R.; Rodrigues, M.; Pezzi, R. P.; Machado, G.; Amaral, L.; Teixeira, S. R.; Weibel, D. E.; Dupont, J.; *J. Braz. Chem. Soc.* **2010**, *21*, 1359.

13. Fujishima, A.; Honda, K.; *Nature* **1972**, *238*, 37.

14. Chamjangali, M. A.; Boroumand, S.; *J. Braz. Chem. Soc.* **2013**, *24*, 1329.

15. Chen, Y.; Dionysiou, D. D.; *Appl. Catal. B: Environ.* **2008**, *80*, 147.

16. Chen, F. T.; Fang, P. F.; Liu, Z.; Gao, Y. P.; Liu, Y.; Dai, Y. Q.; Luo, H.; Feng, J. W.; *J. Mater. Sci.* **2013**, *48*, 5171.

17. Feng, B.; Yang, J. H.; Cao, J.; Yang, L. L.; Gao, M.; Wei, M. B.; Zhai, H. J.; Sun, Y. F.; Song, H.; *J. Alloys Compd.* **2013**, *555*, 241.

18. Liang, H. Y.; Yang, Y. X.; Tang, J. C.; Ge, M.; *Mater. Sci. Semicond. Process.* **2013**, *16*, 1650.

19. Zhang, L.; Yan, J. H.; Zhou, M. J.; Yang, Y. H.; Liu, Y. N.; *Appl. Surf. Sci.* **2013**, *268*, 237.

20. Gui, M. S.; Zhang, W. D.; Su, Q. X.; Chen, C. H.; *J. Solid State Chem.* **2011**, *184*, 1977.

21. Dong, L.; Zhang, X.; Dong, X.; Zhang, X.; Ma, C.; Ma, H.; Xue, M.; Shi, F.; *J. Colloid Interface Sci.* **2013**, *393*, 126.

22. Pare, B.; Sarwan, B.; Jonnalagadda, S. B.; *J. Mol. Struct.* **2012**, *1007*, 196.

23. Xu, J.; Meng, W.; Zhang, Y.; Li, L.; Guo, C.; *Appl. Catal. B: Environ.* **2011**, *107*, 355.

24. Ai, Z.; Huang, Y.; Lee, S.; Zhang, L.; *J. Alloys Compd.* **2011**, *509*, 2044.

25. Zhang, L. S.; Wang, H. L.; Chen, Z. G.; Wong, P. K.; Liu, J. S.; *Appl. Catal. B: Environ.* **2011**, *106*, 1.

26. Zhang, L. W.; Xu, T. G.; Zhao, X.; Zhu, Y. F.; *Appl. Catal. B: Environ.* **2010**, *98*, 138.

27. Ren, L.; Ma, L. L.; Jin, L.; Wang, J. B.; Qiu, M. Q.; Yu, Y.; *Nanotech.* **2009**, *20*, 405602.

28. Yu, J. G.; Xiong, J. F.; Cheng, B.; Yu, Y.; Wang, J. B.; *J. Solid State Chem.* **2005**, *178*, 1968.

29. Ponzoni, C.; Rosa, R.; Cannio, M.; Buscaglia, V.; Finocchio, E.; Nanni, P.; Leonelli, C.; *J. Eur. Ceram. Soc.* **2013**, *33*, 1325.

30. Grice, J. D.; *Can. Mineral.* **2002**, *40*, 693.

31. Madhusudan, P.; Ran, J.; Zhang, J.; Yu, J.; Liu, G.; *Appl. Catal. B: Environ.* **2011**, *110*, 286.

32. Liu, Y. Y.; Wang, Z. Y.; Huang, B. B.; Yang, K. S.; Zhang, X. Y.; Qin, X. Y.; Dai, Y.; *Appl. Surf. Sci.* **2010**, *257*, 172.

33. Marinho, J. Z.; Silva, R. A. B.; Barbosa, T. G. G.; Richter, E. M.; Munoz, R. A. A.; Lima, R. C.; *Electroanalysis* **2013**, *25*, 765.

34. Chen, R.; So, M. H.; Yang, J.; Deng, F.; Che, C. M.; Sun, H. Z.; *Chem. Commun.* **2006**, *21*, 2265.

35. Zhao, T.; Zai, J.; Xu, M.; Zou, Q.; Su, Y.; Wang, K.; Qian, X.; *CrystEngComm* **2011**, *13*, 4010.

36. Madhusudan, P.; Zhang, J.; Cheng, B.; Liu, G.; *CrystEngComm* **2013**, *15*, 231.

37. Chen, L.; Huang, R.; Yin, S.-F.; Luo, S.-L.; Au, C.-T.; *Chem. Eng. J.* **2012**, *193*, 123.

38. Cheng, H.; Huang, B.; Yang, K.; Wang, Z.; Qin, X.; Zhang, X.; Dai, Y.; *ChemPhysChem* **2010**, *11*, 2167.

39. Komarneni, S.; Roy, R.; Li, Q. H.; *Mater. Res. Bull.* **1992**, *27*, 1393.

40. de Moura, A. P.; Lima, R. C.; Paris, E. C.; Li, M. S.; Varela, J. A.; Longo, E.; *J. Solid State Chem.* **2011**, *184*, 2818.

41. Hu, X. L.; Yu, J. C.; *Adv. Funct. Mater.* **2008**, *18*, 880.

42. de Moura, A. P.; Lima, R. C.; Moreira, M. L.; Volanti, D. P.; Espinosa, J. W. M.; Orlandi, M. O.; Pizani, P. S.; Varela, J. A.; Longo, E.; *Solid State Ionics* **2010**, *181*, 775.

43. Komarneni, S.; Katsuki, H.; *Ceram. Int.* **2010**, *36*, 1165.

44. Volanti, D. P.; Keyson, D.; Cavalcante, L. S.; Simoes, A. Z.; Joya, M. R.; Longo, E.; Varela, J. A.; Pizani, P. S.; Souza, A. G.; *J. Alloys Compd.* **2008**, *459*, 537.

45. Comissão Nacional de Normas e Padrões para Alimentos (CNNPA); Resolução No. 44: Brasília, Brasil,1977.

46. U.S. Food and Drug Administration (FDA); Compliance Program Guidance Manual. In http://www.fda.gov/downloads/Food/GuidanceComplianceRegulatoryInformation/ComplianceEnforcement/ucm073305.pdf accessed in December 2014.

47. European Food Safety Authority (EFSA); *Scientific Opinion on the Re-evaluation of Ponceau 4R (E 124) as a Food Additive*. In http://www.efsa.europa.eu/en/scdocs/scdoc/1328.htm accessed in December 2014.

48. Hernandez-Martinez, A. R.; Estevez, M.; Vargas, S.; Rodriguez, R.; *Compos. Part. B-Eng.* **2013**, *44*, 686.

49. Salem, M. A.; Abdel-Halim, S. T.; El-Sawy, A.; Zaki, A. B.; *Chemosphere* **2009**, *76*, 1088.

50. Palfi, T.; Wojnarovits, L.; Takacs, E.; *Radiat. Phys. Chem.* **2011**, *80*, 462.

51. Kieke, M. L.; Schoppelrei, J. W.; Brill, T. B.; *J. Phys. Chem.* **1996**, *100*, 7455.

52. Marinho, J. Z.; Romeiro, F. C.; Lemos, S. C. S.; Motta, F. V.; Riccardi, C. S.; Li, M. S.; Longo, E.; Lima, R. C.; *J. Nanomater.* **2012**, *2012*, 1.

53. Riccardi, C. S.; Lima, R. C.; dos Santos, M. L.; Bueno, P. R.; Varela, J. A.; Longo, E.; *Solid State Ionics* **2009**, *180*, 288.

54. Wang, H. C.; Lu, C. H.; *Mater. Res. Bull.* **2002**, *37*, 783.

55. Patterson, E. M.; Shelden, C. E.; Stockton, B. H.; *Appl. Opt.* **1977**, *16*, 729.

56. Zhang, X. C.; Guo, T. Y.; Wang, X. W.; Wang, Y. W.; Fan, C. M.; Zhang, H.; *Appl. Catal. B: Environ.* **2014**, *150*, 486.

57. Hou, J.; Yang, C.; Wang, Z.; Zhou, W.; Jiao, S.; Zhu, H.; *Appl. Catal. B: Environ.* **2013**, *142*, 504.

58. Tsuji, M.; Ikeda, Y.; Sazarashi, M.; Yamaguchi, M.; Matsunami, J.; Tamaura, Y.; *Mater. Res. Bull.* **2000**, *35*, 2109.

59. Wang, C. J.; Zhao, Z. W.; Luo, B.; Fu, M.; Dong, F.; *J. Nanomater.* **2014**, *2014*, 1.

60. Sun, Y. Y.; Wang, W. Z.; Zhang, L.; Zhang, Z. J.; *Chem. Eng. J.* **2012**, *211*, 161.

61. Wang, Y.; Wen, Y. Y.; Ding, H. M.; Shan, Y. K.; *J. Mater. Sci.* **2010**, *45*, 1385.

62. Taylor, P.; Sunder, S.; Lopata, V. J.; *Can. J. Chem.* **1984**, *62*, 2863.

63. Dong, F.; Lee, S. C.; Wu, Z. B.; Huang, Y.; Fu, M.; Ho, W. K.; Zou, S. C.; Wang, B.; *J. Hazard. Mater.* **2011**, *195*, 346.

64. Narang, S. N.; Patel, N. D.; Kartha, V. B.; *J. Mol. Struct.* **1994**, *327*, 221.

65. Yang, H.; Li, G. Y.; An, T. C.; Gao, Y. P.; Fu, J. M.; *Catal. Today* **2010**, *153*, 200.

66. Zheng, Y.; Duan, F.; Chen, M.; Xie, Y.; *J. Mol. Catal. A: Chem.* **2010**, *317*, 34.

67. Cai, G. Y.; Xu, L. L.; Wei, B.; Che, J. X.; Gao, H.; Sun, W. J.; *Mater. Lett.* **2014**, *120*, 1.